Biomedical Signal Processing and Control 8 (2013) 779–791

Contents lists available at ScienceDirect

Biomedical Signal Processing and Control

journal homepage: www.elsevier.com/locate/bspc

MRI denoising using nonlocal neutrosophic set approach of Wiener filtering

J. Mohan [a,*], V. Krishnaveni [b], Yanhui Guo [c]

[a] Department of Electronics and Communication Engineering, P.A. College of Engineering and Technology, Pollachi 642 002, Tamilnadu, India
[b] Department of Electronics and Communication Engineering, PSG College of Technology, Coimbatore 641 004, Tamilnadu, India
[c] School of Science, Technology and Engineering Management, Saint Thomas University, Miami Gardens, FL 33054, USA

ARTICLE INFO

Article history:
Received 11 February 2013
Received in revised form 6 July 2013
Accepted 19 July 2013
Available online 22 August 2013

Keywords:
Denoising
Magnetic resonance imaging
Neutrosophic set
Nonlocal means
PSNR
Rician distribution
SSIM
Wiener

ABSTRACT

In this paper, a new filtering method is presented to remove the Rician noise from magnetic resonance images (MRI) acquired using single coil MRI acquisition system. This filter is based on nonlocal neutrosophic set (NLNS) approach of Wiener filtering. A neutrosophic set (NS), a part of neutrosophy theory, studies the origin, nature, and scope of neutralities, as well as their interactions with different ideational spectra. Now, we apply the neutrosophic set into image domain and define some concepts and operators for image denoising. First, the nonlocal mean is applied to the noisy MRI. The resultant image is transformed into NS domain, described using three membership sets: true (T), indeterminacy (I) and false (F). The entropy of the neutrosophic set is defined and employed to measure the indeterminacy. The ω-Wiener filtering operation is used on T and F to decrease the set indeterminacy and to remove the noise. The experiments have been conducted on simulated MR images from Brainweb database and clinical MR images. The results show that the NLNS Wiener filter produces better denoising results in terms of qualitative and quantitative measures compared with other denoising methods, such as classical Wiener filter, the anisotropic diffusion filter, the total variation minimization and the nonlocal means filter. The visual and the diagnostic quality of the denoised image are well preserved.

1. Introduction

Magnetic resonance imaging (MRI) is a powerful diagnostic technique used in radiology to visualize detailed internal structures of the human body. MRI is primarily used to demonstrate pathological or other physiological alterations of living tissues and is a commonly used form of medical imaging [1]. Despite significant improvements in recent years, MR images often suffer from low signal to noise ratio (SNR) especially in cardiac and brain imaging [2]. This is problematic for further tasks such as segmentation of important features; classification of images for computer aided diagnostics, three dimensional image reconstruction and image registration. Therefore, it is important to improve the SNR of the images used during quantitative analysis. This is usually done by using a denoising method, which is an important preprocessing step used to improve the image quality by reducing the noise component while preserving all the image features.

Numerous approaches of denoising MR images have been proposed in the literatures. Henkelman [3] was the first to estimate the magnitude MR image from a noisy image. McVeigh et al. [4] proposed the spatial filtering and temporal filtering for reducing Gaussian noise in MR images. These filters eliminate the high frequency noise at the expense of blurring fine details and sharp edges in the MR images. A large number of edge-preserving methods have been proposed to overcome the above-mentioned blurring effects. For example, anisotropic diffusion filtering of MRI denoising proposed by Gerig et al. [5] are able to remove noise using gradient information while respecting important image structures. Recently, Krissian and Aja-Fernandez [6] proposed a new anisotropic diffusion filter based on a linear minimum mean squared error estimation and partial difference equations for Rician noise removal that has achieved state-of-the-art results. Samsonov and Johnson [7] proposed the noise adaptive non-linear diffusion method for filtering MR images with spatially varying noise levels. By using the receiver coil sensitivity profiles, the priori information regarding the image noise level spatial distribution is obtained and it is utilized for the local adjustment of the anisotropic diffusion filter.

A simple wavelet based noise reduction was proposed by Weaver et al. [8]. The main drawback of the method was small

Abbreviations: ADF, anisotropic diffusion filter; MRI, magnetic resonance imaging; NLM, nonlocal means; NLNS, nonlocal neutrosophic set; NS, neutrosophic set; PSNR, peak signal to noise ratio; SNR, signal to noise ratio; SSIM, structural similarity index; TV, total variation.

* Corresponding author. Tel.: +91 98 407 13417.
E-mail addresses: jaimohan12@gmail.com (J. Mohan), vk@ece.psgtech.ac.in (V. Krishnaveni), yguo@stu.edu (Y. Guo).

1746-8094/$ – see front matter © 2013 Elsevier Ltd. All rights reserved.
http://dx.doi.org/10.1016/j.bspc.2013.07.005

structures similar in size to noise were also eliminated. Wavelet transform based denoising for Rician noise removal in MRI was proposed by Nowak [9]. Pizurica et al. [10] proposed an alternative for denoising MR images with Rician noise using low complexity joint detection and estimation method. In the squared magnitude of the MR image, introduce an analytical model for the probability of signal presence, which is adapted to the global coefficients histogram and to a local indicator of spatial activity (locally averaged magnitude of the wavelet coefficients). Subtract the constant bias from the scaling coefficients, and subsequently compute the square root of the denoised squared-magnitude image.

Bao and Zang [11] proposed a MR image denoising method based on an adaptive multiscale products threshold which incorporates the merits of interscale dependencies into the thresholding technique for denoising. Two adjacent wavelet subbands are multiplied to amplify the significant features and to dilute the noise. Apply thresholding to the multiscale products instead of the wavelet coefficients to better differentiate edge structures for noise. The distribution of the products analyzed and an adaptive threshold is formulated to remove most of the noise. Thus, it is a good edge preserving denoising method. Yang and Fei [12] proposed the wavelet multiscale denoising method for the Rician nature of MR data. In this method, Radon transform is applied to the original MR images and the Gaussian noise model is used to process the MR sinogram image. A translation invariant wavelet transform is employed to decompose the MR sinogram into multiscales in order to effectively denoise the image.

Nonlocal means (NLM) filter introduced by Buades et al. [13] has emerged as a very simple and effective way to reduce noise while minimally affecting the original structures of the image. Manjon et al. [14] modified the original NLM algorithm to denoise the multispectral MRI. In the multispectral sequences, the similarity measure can be obtained by combining information of various channels. Manjon et al. [15] proposed the unbiased NLM approach for MRI denoising. The unbiased NLM is obtained by subtracting the noise bias from the squared value of NLM. The main drawback of the NLM algorithm is computational burden due to its complexity especially on 3D MRI data. In order to overcome this, Coupe et al. [16] proposed an optimized blockwise NLM filter for denoising 3D MRI. This is achieved by the following steps: an automatic tuning of the smoothing parameter, a selection of the most relevant voxels for NL means computation, a blockwise implementation and a parallelized computation. Manjon et al. [17] proposed the denoising methods for three-dimensional MR images by exploiting the sparseness and self-similarity properties of the images. These methods are based on a three-dimensional moving window cosine transform hard thresholding and a three-dimensional rotationally invariant version of the NLM filter.

Sijbers et al. [18–20] estimated the Rician noise level and performed signal reconstruction using maximum likelihood (ML) approach for reducing bias that appears in the conventional approach. Sijbers et al. [21] used this approach to estimate the image noise variance from the background mode of the histogram of MR image which is known to be Rayleigh distributed. He and Greenshields [22] used the nonlocal maximum likelihood (NLML) estimation method for Rician noise. This method is based on deploying maximum likelihood estimator on the nonlocal neighborhood in order to predict the underlying noise. Rajan et al. [23] used the ML based estimation of the local variance for each pixel of the image using a local neighborhood when no background information is available, like cardiac and lung images. Rajan et al. [24] proposed the MRI denoising for spatially varying noise levels based on ML estimation using restricted local neighborhoods. Recently, Rajan et al. [25] presented nonlocal maximum likelihood estimation for denoising multiple coil MR images.

This paper focuses on developing a new denoising method based on the nonlocal neutrosophic set (NLNS) approach of Wiener filtering to remove the Rician noise in MRI. First the NLM method is applied to the noisy MRI and the resultant image is transformed into the neutrosophic set. The ω-Wiener filtering is employed to reduce the indetermination degree of the image, which is measured by the entropy of the indeterminate subset, after filtering, the noise is removed. The rest of this paper is organized as follows: Section 2 discusses the characteristics of the noise in MRI. In Section 3, the proposed methodology of MRI denoising is described in detail. The materials used to evaluate the performance of the proposed method, the validation strategies and the comparative evaluation of the denoising results are discussed in Section 4. Section 5 presents the conclusion and the future scope.

2. Characteristics of the noise in MRI

The raw data obtained during MRI scanning are complex values that represent the Fourier transform of a magnetization distribution of a volume of tissue at a certain point of time. An inverse Fourier transform converts these raw data into magnitude, frequency and phase components that more directly represent the physiological and morphological features of interest in the person being scanned. So, noise in the *k*-space in MR data from each coil is assumed to be a zero mean uncorrelated Gaussian process with equal variance in both real and imaginary parts because of the linearity and orthogonality of the Fourier transform. However, it is common practice to transform the complex valued images into magnitude and phase images. Since computation of a magnitude (or phase) image is a nonlinear operation, the probability density function (PDF) of the data under concern changes. The magnitude data in spatial domain is modeled as the Rician distribution and the so-called Rician noise (the error between the underlying image intensities and the measurement data) is locally signal dependent [26].

The complex MR data is given as,

$$M = a + ib \tag{1}$$

The noise added to the complex raw data is zero mean Gaussian noise $N(0, \sigma^2)$,

$$M = (a + n_{re}) + i(b + n_{im}) \tag{2}$$

The spatial MR image is the magnitude of the noisy raw data. Therefore,

$$|M| = \sqrt{(a + n_{re})^2 + (b + n_{im})^2} \tag{3}$$

Thus, the distribution of $|M|$ becomes Rician [23] and is represented as,

$$p_M(M \,|A, \sigma_n) = \frac{M}{\sigma_n^2} e^{-(M^2+A^2)/2\sigma_n^2} I_0\left(\frac{AM}{\sigma_n^2}\right) u(M) \tag{4}$$

with $I_0(\cdot)$ as the modified zeroth order Bessel function of the first kind, σ_n^2 is the noise variance, A is the noiseless signal level, M is the MR magnitude variable and $u(\cdot)$ the Heaviside step function. In high SNR, i.e., high intensity (bright) regions of the magnitude image, the Rician distribution tends to a Gaussian distribution with mean $\sqrt{A^2 + \sigma_n^2}$ and variance σ_n^2 given as

$$p_M(M \,|A, \sigma_n) \approx \frac{1}{\sqrt{2\pi\sigma_n^2}} e^{-(M^2 - \sqrt{A^2+\sigma_n^2})/2\sigma_n^2} u(M) \tag{5}$$

In the image background, where SNR is zero due to the lack of water proton density in the air, the Rician PDF simplifies to a Rayleigh distribution with PDF

$$p_M(M,\sigma_n) = \frac{M}{\sigma_n^2} e^{-(M^2/2\sigma_n^2)} u(M) \tag{6}$$

Thus, Rician noise in MR images behaves to be Gaussian distributed when SNR is high and Rayleigh distributed for low SNR. The squared magnitude image (the value of each pixel in the image is the square of the value of the corresponding pixel in the original magnitude image) has a noise bias which is signal independent and it can be easily removed. Such bias is equal to $2\sigma^2$ as shown by Nowak [9] and therefore, a simple bias subtraction will recover its original value. The estimation of the noise standard deviation σ from the noisy MR image is based on the local estimation of the skewness of the magnitude data distribution proposed by Rajan et al. [23].

3. Proposed methods

Neutrosophy, a branch of philosophy introduced in [27] as a generalization of dialectics, studies the origin, nature and scope of neutralities, as well as their interactions with different ideational spectra. In neutrosophy theory, every event has not only a certain degree of the truth, but also a falsity degree and an indeterminacy degree that have to be considered independently from each other [27]. Thus, a theory, event, concept, or entity, {*S*} is considered with its opposite {Anti-*S*} and the neutrality {Neut-*S*}. {Neut-*S*} is neither {*S*} nor {Anti-*S*}. The {Neut-*S*} and {Anti-*S*} are referred to as {Non-*S*}. According to this theory, every idea {*S*} is neutralized and balanced by {Anti-*S*} and {Non-*S*} [27]. Neutrosophic set (NS) provides a powerful tool to deal with indeterminacy.

NS had been applied to image thresholding, image segmentation and image denoising applications [28–32]. Cheng and Guo [28] proposed a thresholding algorithm based on neutrosophy, which could select the thresholds automatically and effectively. The NS approach of image segmentation for real images [29] and for color texture image segmentation discussed in [30]. In [31], some concepts and operators were defined based on NS and applied for image denoising. It can process not only noisy images with different levels of noise, but also images with different kinds of noise well. The method proposed in [31] adapted and applied for MRI denoising [32], which shows some significant improvement in denoising. This paper is presented as an extended work of [33]; MRI denoising based on NLNS based Wiener filtering is evaluated with Simulated and clinical MR images. Since the NLM filtered image is used as the reference image for NS domain to reduce the indeterminacy of the sets, this method is suitable for denoising MR images with Rician noise.

3.1. Nonlocal means operation

The NLM method is applied to the noisy MRI in order to create the reference image. In the nonlocal means [13], Given a discrete noisy image $u = \{u(i) \,|\, i \in I\}$, the estimated value $NL[u](i)$, for a pixel i, is computed as a weighted average of all the pixels in the image,

$$NL[u](i) = \sum_{j \in I} w(i,j) u(j) \tag{7}$$

where the family of weights $\{w(i,j)\}_j$ depends on the similarity between the pixels i and j, and satisfy the usual conditions $0 \le w(i,j) \le 1$ and $\sum_j w(i,j) = 1$.

The similarity between two pixels i and j depends on the similarity of the intensity gray level vectors $u(N_i)$ and $u(N_j)$, where N_k denotes a square neighborhood of fixed size and centered at a pixel k. This similarity is measured as a decreasing function of the weighted Euclidean distance, $\left\|u(N_i) - u(N_j)\right\|_{2,a}^2$, where $a > 0$ is the standard deviation of the Gaussian kernel. The application of the Euclidean distance to the noisy neighborhoods raises the following equality

$$E\left\|u(N_i) - u(N_j)\right\|_{2,a}^2 = \left\|u(N_i) - u(N_j)\right\|_{2,a}^2 + 2a^2 \tag{8}$$

This equality shows the robustness of the algorithm since in expectation the Euclidean distance conserves the order of similarity between pixels.

The pixels with a similar gray level neighborhood to $u(N_i)$ have larger weights in the average. These weights are defined as,

$$w(i,j) = \frac{1}{Z(i)} e^{-\left\|u(N_i) - u(N_j)\right\|_{2,a}^2 / h^2} \tag{9}$$

where $Z(i)$ is the normalizing constant.

$$Z(i) = \sum_j e^{-\left\|u(N_i) - u(N_j)\right\|_{2,a}^2 / h^2} \tag{10}$$

and the parameter h acts as a degree of filtering. It controls the decay of the exponential function and therefore the decay of the weights as a function of the Euclidean distances.

3.2. The image in neutrosophic set

The NLM filtered image is transformed into NS domain. A neutrosophic set image P_{NS} is characterized by three membership sets *T*,*I*,*F*. A pixel *P* in the image is described as *P*(*T*,*I*,*F*) and belongs to *W* in the following way: it is *t* true in the set, *i* indeterminate in the set, and *f* false in the set, where *t* varies in *T*, *i* varies in *I* and *f* varies in *F*. Then the pixel *P*(*i*,*j*) in the image domain is transformed into the neutrosophic set domain $P_{NS}(i,j) = \{T(i,j), I(i,j), F(i,j)\}$. $T(i,j)$, $I(i,j)$ and $F(i,j)$ are the probabilities belong to white pixels set, indeterminate set and non white pixels set, respectively [31–33], which are defined as:

$$T(i,j) = \frac{\bar{g}(i,j) - \bar{g}_{\min}}{\bar{g}_{\max} - \bar{g}_{\min}} \tag{11}$$

$$\bar{g}(i,j) = \frac{1}{w \times w} \sum_{m=i-w/2}^{i+w/2} \sum_{n=j-w/2}^{j+w/2} g(m,n) \tag{12}$$

$$I(i,j) = \frac{\delta(i,j) - \delta_{\min}}{\delta_{\max} - \delta_{\min}} \tag{13}$$

$$\delta(i,j) = abs(g(i,j) - \bar{g}(i,j)) \tag{14}$$

$$F(i,j) = 1 - T(i,j) \tag{15}$$

where $\bar{g}(i,j)$ is the local mean value of the pixels of the window. $\delta(i,j)$ is the absolute value of difference between intensity $g(i,j)$ and its local mean value $\bar{g}(i,j)$.

3.3. Neutrosophic image entropy

For an image, the entropy is utilized to evaluate the distribution of the gray levels. If the entropy is maxim, the intensities have equal probability. If the entropy is small, the intensity distribution is non-uniform.

Neutrosophic entropy of an image is defined as the summation of the entropies of three subsets *T*, *I* and *F* [31–33]:

$$En_{NS} = En_T + En_I + En_F \tag{16}$$

$$En_T = -\sum_{a=\min\{T\}}^{\max\{T\}} p_T(a)\ln p_T(a) \tag{17}$$

$$En_I = -\sum_{a=\min\{I\}}^{\max\{I\}} p_I(a)\ln p_I(a) \tag{18}$$

$$En_F = -\sum_{a=\min\{F\}}^{\max\{F\}} p_F(a)\ln p_F(a) \tag{19}$$

where En_T, En_I and En_F are the entropies of sets T, I and F, respectively. $p_T(a)$, $p_I(a)$ and $p_F(a)$ are the probabilities of elements in T, I and F, respectively.

3.4. ω-Wiener filtering operation

The values of $I(i,j)$ are employed to measure the indeterminate degree of element $P_{NS}(i,j)$. To make the set I correlated with T and F, the changes in T and F influence the distribution of element in I and vary the entropy of I. A ω-Wiener filtering operation *for* P_{NS}, $\hat{P}_{NS}(\omega)$, is defined as [33]:

$$\hat{P}_{NS}(\omega) = P(\hat{T}(\omega), \hat{I}(\omega), \hat{F}(\omega)) \tag{20}$$

$$\hat{T}(\omega) = \begin{cases} T & I < \omega \\ \hat{T}_\omega & I \geq \omega \end{cases} \tag{21}$$

$$\hat{T}_\omega(i,j) = \underset{(m,n)\in S_{i,j}}{\text{wiener}}\{T(m,n)\} \tag{22}$$

$$\hat{F}(\omega) = \begin{cases} F & I < \omega \\ \hat{F}_\omega & I \geq \omega \end{cases} \tag{23}$$

$$\hat{F}_\omega(i,j) = \underset{(m,n)\in S_{i,j}}{\text{wiener}}\{F(m,n)\} \tag{24}$$

$$\hat{I}_\omega(i,j) = \frac{\delta_{\hat{T}}(i,j) - \delta_{\hat{T}\min}}{\delta_{\hat{T}\max} - \delta_{\hat{T}\min}} \tag{25}$$

$$\delta_{\hat{T}}(i,j) = abs(\hat{T}(i,j) - \bar{\hat{T}}(i,j)) \tag{26}$$

$$\bar{\hat{T}}(i,j) = \frac{1}{w\times w}\sum_{m=i-w/2}^{i+w/2}\sum_{n=j-w/2}^{j+w/2} \hat{T}(m,n) \tag{27}$$

where $\delta_{\hat{T}}(i,j)$ is the absolute value of difference between intensity $\hat{T}(i,j)$ and its local mean value $\bar{\hat{T}}(i,j)$ at (i,j) after ω-Wiener filtering operation.

After new concepts and operators are defined in the neutrosophic set for an image, a MRI denoising method based on nonlocal neutrosophic set approach of Wiener filtering is proposed and summarized as below (see Fig. 1):

(1) NLM algorithm is applied to the noisy MRI;
(2) Transform the resultant image into NS domain;
(3) Use ω-Wiener filtering operation on the true subset T to obtain T_ω;
(4) Compute the entropy of the indeterminate subset $\hat{I}_\omega$, $En_{\hat{I}_\omega}(i)$;
(5) if $((En_{\hat{I}_\omega}(i+1) - En_{\hat{I}_\omega}(i))/En_{\hat{I}_\omega}(i)) < \delta$, go to Step 5; else $T = \hat{T}_\omega$, go to Step 2;
(6) Transform subset $\hat{T}_\omega$ from the neutrosophic domain into the gray level domain.

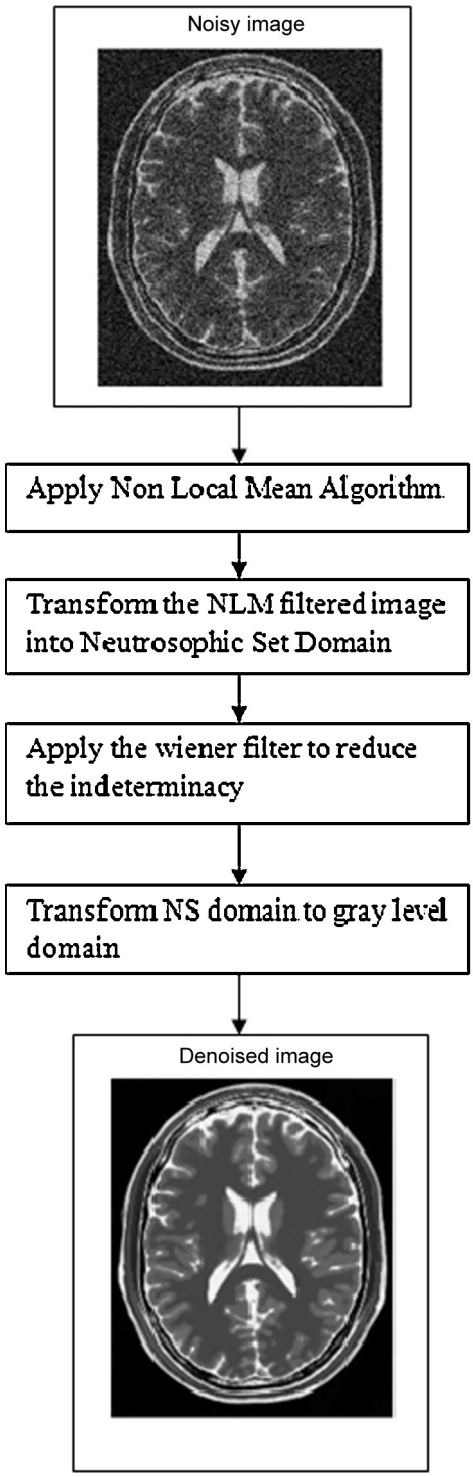

Fig. 1. Block diagram of the MRI denoising method based on NLNS Wiener filtering.

4. Experimental results and discussions

4.1. Materials

The experiments were conducted on two MRI datasets. The first data set consists of simulated MR images obtained from the Brainweb database [34]. The second data set consists of clinical MRI collected from PSG Institute of Medical Sciences and Research (PSG IMS & R), Coimbatore, Tamilnadu, India. Simulated MR images are used collectively as the reference to evaluate and compare the

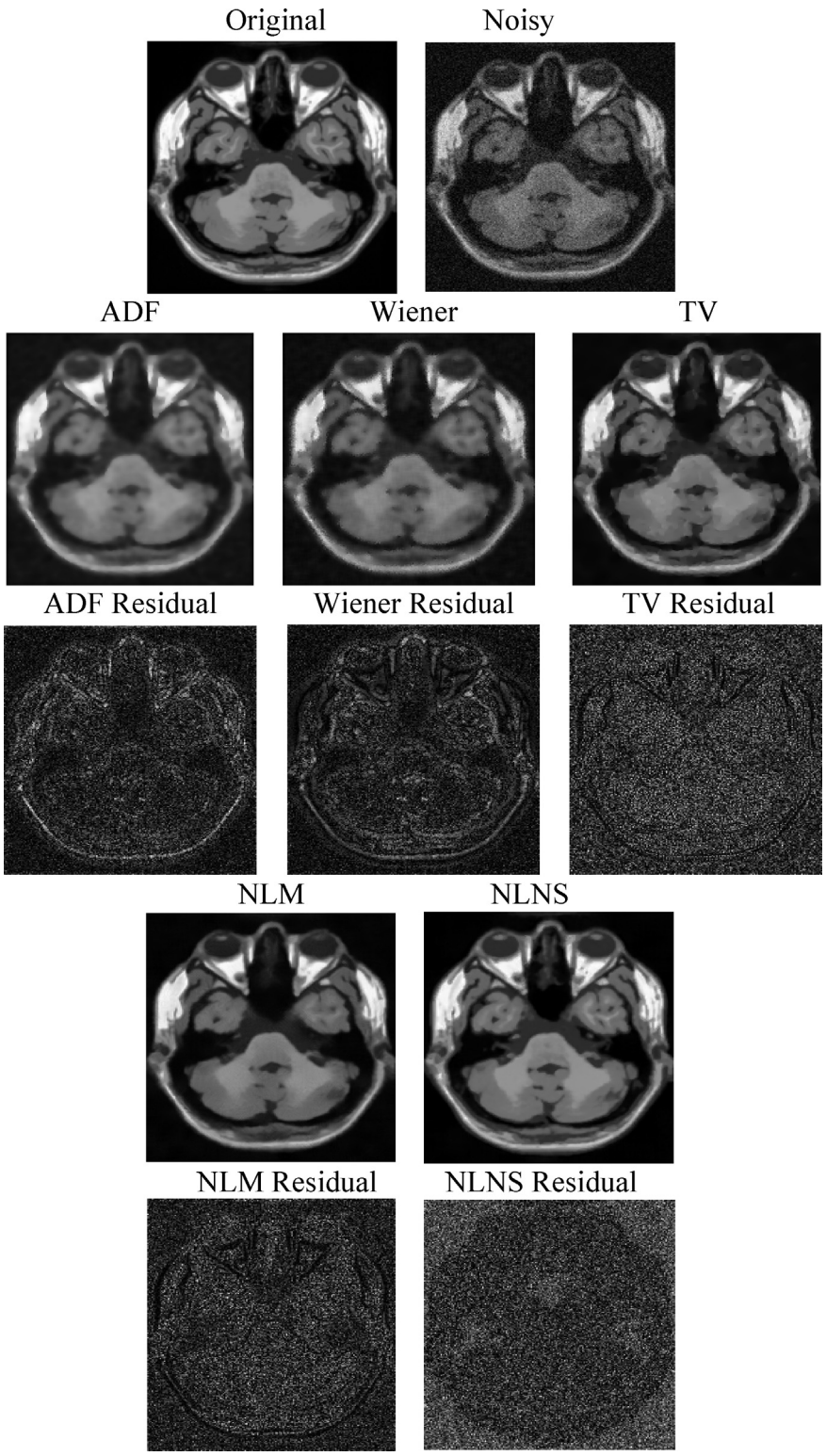

Fig. 2. Denoising results and the corresponding absolute value of residuals for simulated T1 weighted axial MRI corrupted by 7% of Rician noise.

validity of the proposed technique. It evicts the data dependency enabling precise comparative studies. The data set consists of T1 weighted Axial, T2 weighted Axial and T1 weighted Axial with multiple sclerosis (MS) lesion volumes of $181 \times 217 \times 181$ voxels (voxels resolution is $1\,mm^3$), which are corrupted with different level of Rician noise (1% ($\sigma = 2.5$) to 15% ($\sigma = 37.5$) of maximum intensity). Rician noise was generated by Gaussian noise to real and imaginary parts and then computing the magnitude of the image.

In the clinical data sets, the images were acquired using Siemens Magnetom Avanto 1.5 T Scanner and Hitachi 0.3 T AIRIS II scanner. MRI pulse sequences are pattern of radiofrequency pulses and magnetic gradients that are used to produce an image. Here, the images

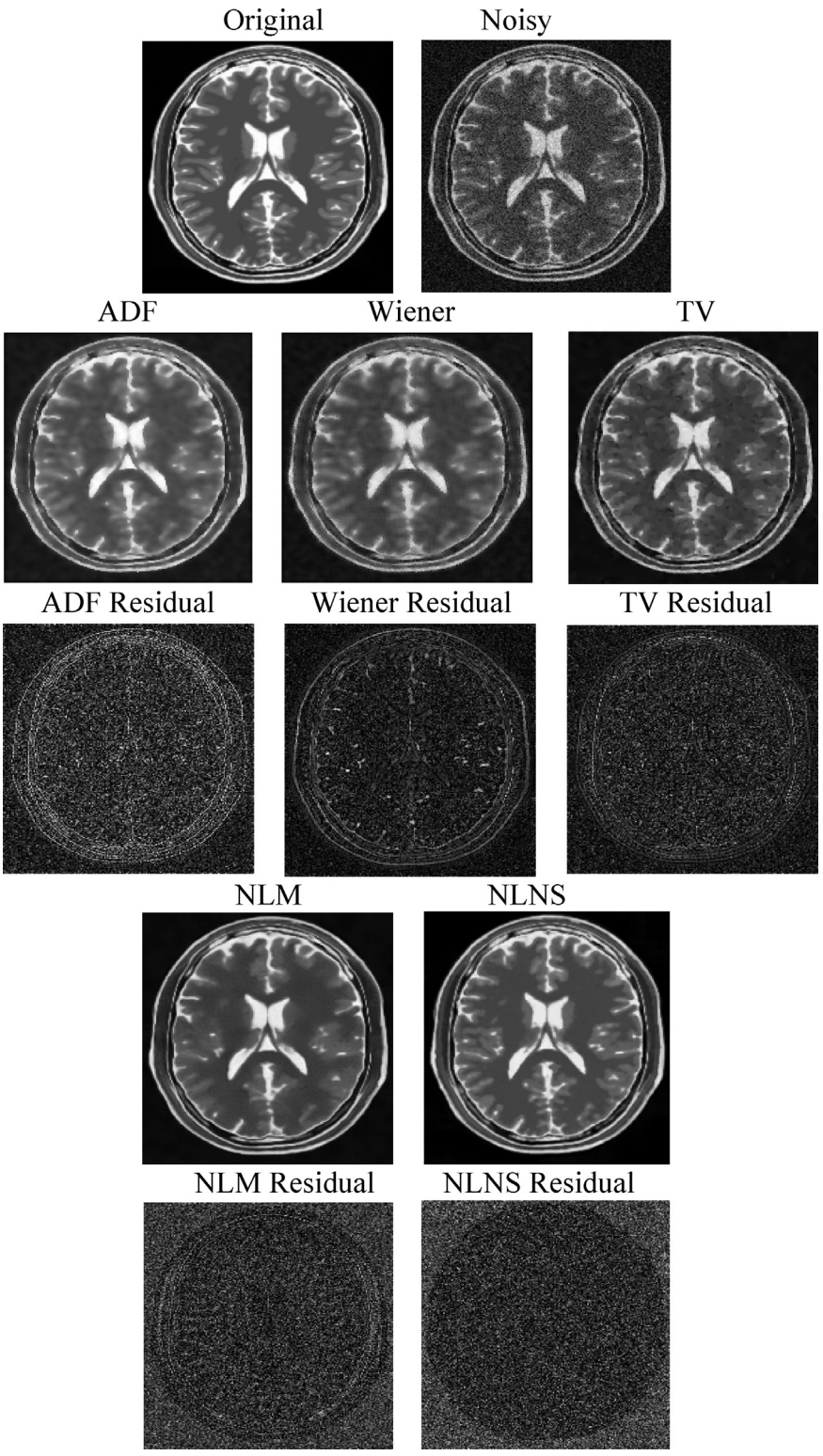

Fig. 3. Denoising results and the corresponding absolute value of residuals for simulated T2 weighted axial MRI corrupted by 9% of Rician noise.

are acquired using spin echo sequences with long repetition time (TR) and short echo time (TE).

1. Siemens Magnetom Avanto 1.5 T Scanner
   a. T2 weighted Sagittal MR image of normal brain with TR = 4460 ms, TE = 85 ms, 5 mm thickness and 512 × 512 resolution.
   b. T1 weighted Axial MR image of tumor pathology with TR = 550 ms, TE = 8.7 ms, 5 mm thickness and 499 × 559 resolution.
2. Hitachi 0.3 T AIRIS II Scanner
   a. T1 weighted Axial MR image of tumor pathology with TR = 249 ms, TE = 18 ms, 6.5 mm thickness and 256 × 256 resolution.

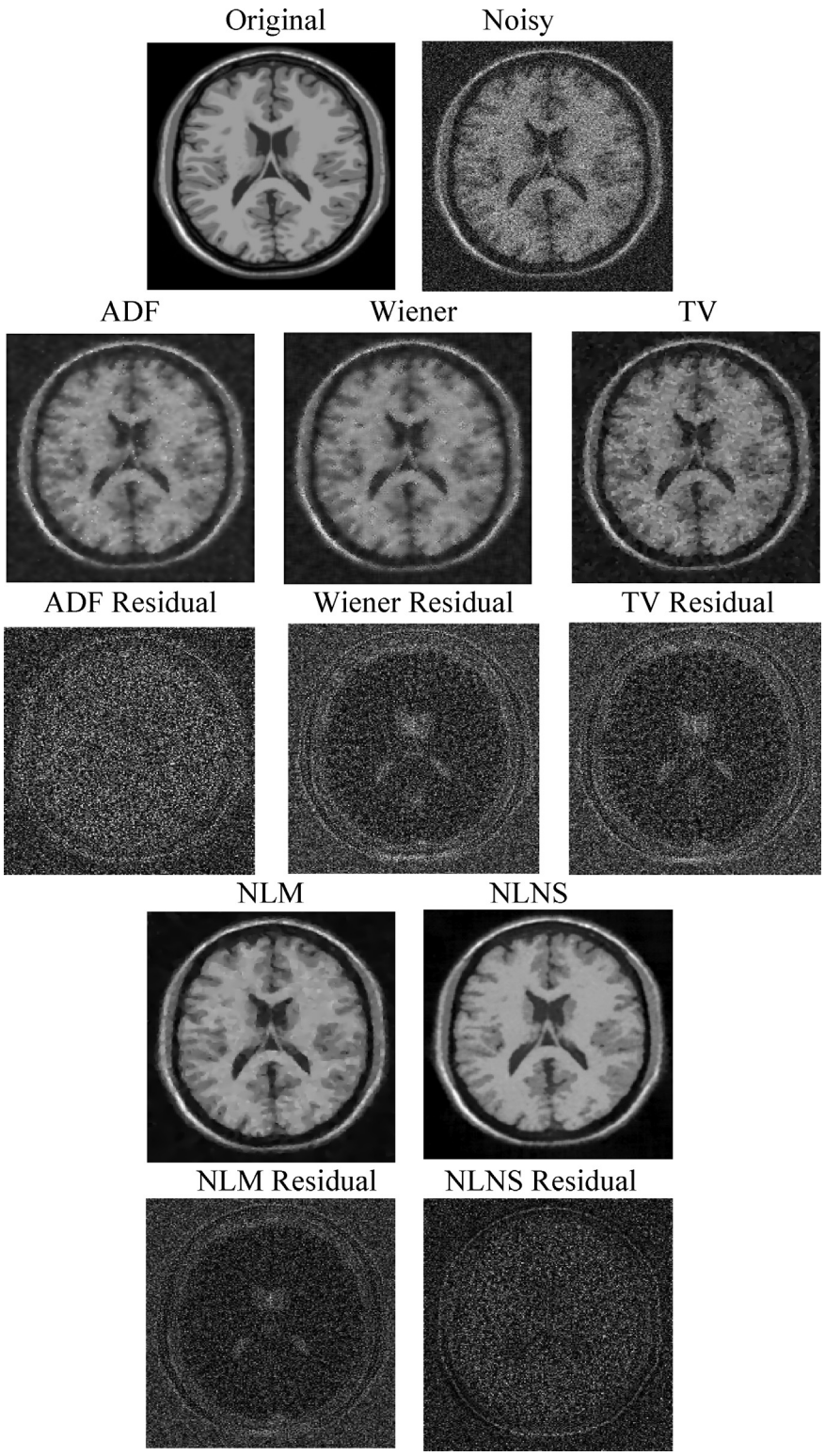

Fig. 4. Denoising results and the corresponding absolute value of residuals for simulated T1 weighted axial MRI with MS lesion corrupted by 15% of Rician noise.

b. T2 weighted Coronal MR image of normal brain with TR = 5472 ms, TE = 125 ms, 7 mm thickness and $256 \times 256 \times 18$ resolution.

4.2. Validation strategies

The performance of the denoising algorithm is measured by using the quality metrics such as peak-signal-to-noise ratio (PSNR), the structural similarity (SSIM) index [35]. The peak signal to noise ratio in decibel (dB) is measured using the following formula:

$$\mathrm{PSNR} = -10 \log_{10} \left[\frac{\sum_{i=0}^{i=H-1} \sum_{j=0}^{j=W-1} (I(i,j) - I_d(i,j))^2}{H \times W \times 255^2} \right] \quad (28)$$

where $I(i, j)$ and $I_d(i, j)$ represent the intensities of pixels (i, j) in the original image and denoised image, respectively. The higher

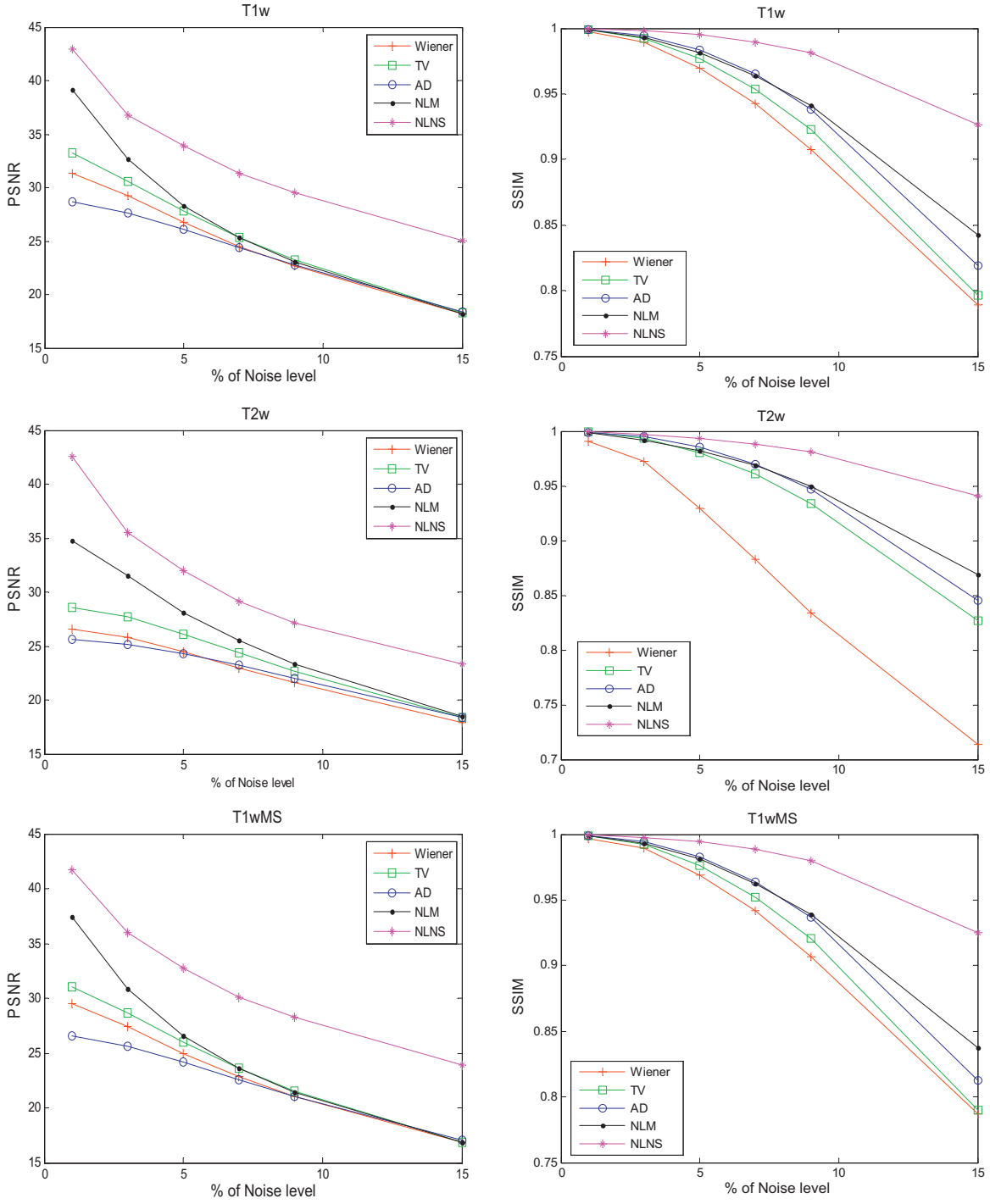

Fig. 5. Comparison results for Brainweb simulated MR images. (Left) PSNR of the compared methods for different image types and noise levels. (Right) SSIM of the compared methods for different image types and noise levels.

the PSNR, the better the denoising algorithm is. SSIM gives the measure of the structural similarity between the original and the denoised images and are in the range of 0 to 1. The SSIM works as follows: let x and y be two non negative images, where as one has perfect quality. Then, the SSIM can serve as a quantitative measure of the similarity of the second image. The system separates the task of similarity measurement into three comparisons: luminance, contrast and structure. It can be defined as

$$\mathrm{SSIM}(x,y) = \frac{(2\mu_x\mu_y + C_1)(2\sigma_{xy} + C_2)}{(\mu_x^2 + \mu_y^2 + C_1)(\sigma_x^2 + \sigma_y^2 + C_2)} \tag{29}$$

where μ_x and μ_y are the estimated mean intensity and σ_x and σ_y are the standard deviations, respectively. σ_{xy} can be estimated as

$$\sigma_{xy} = \frac{1}{N-1}\sum_{i=1}^{N}(x_i - \mu_x)(y_i - \mu_y) \tag{30}$$

C_1 and C_2 in Eq. (29) are constants and the values are given as $C_1 = (K_1L)^2$ and $C_2 = (K_2L)^2$ where $K_1, K_2 \ll 1$ is a small constant and L is the dynamic range of the pixel values (255 for 8 bit gray scale images).

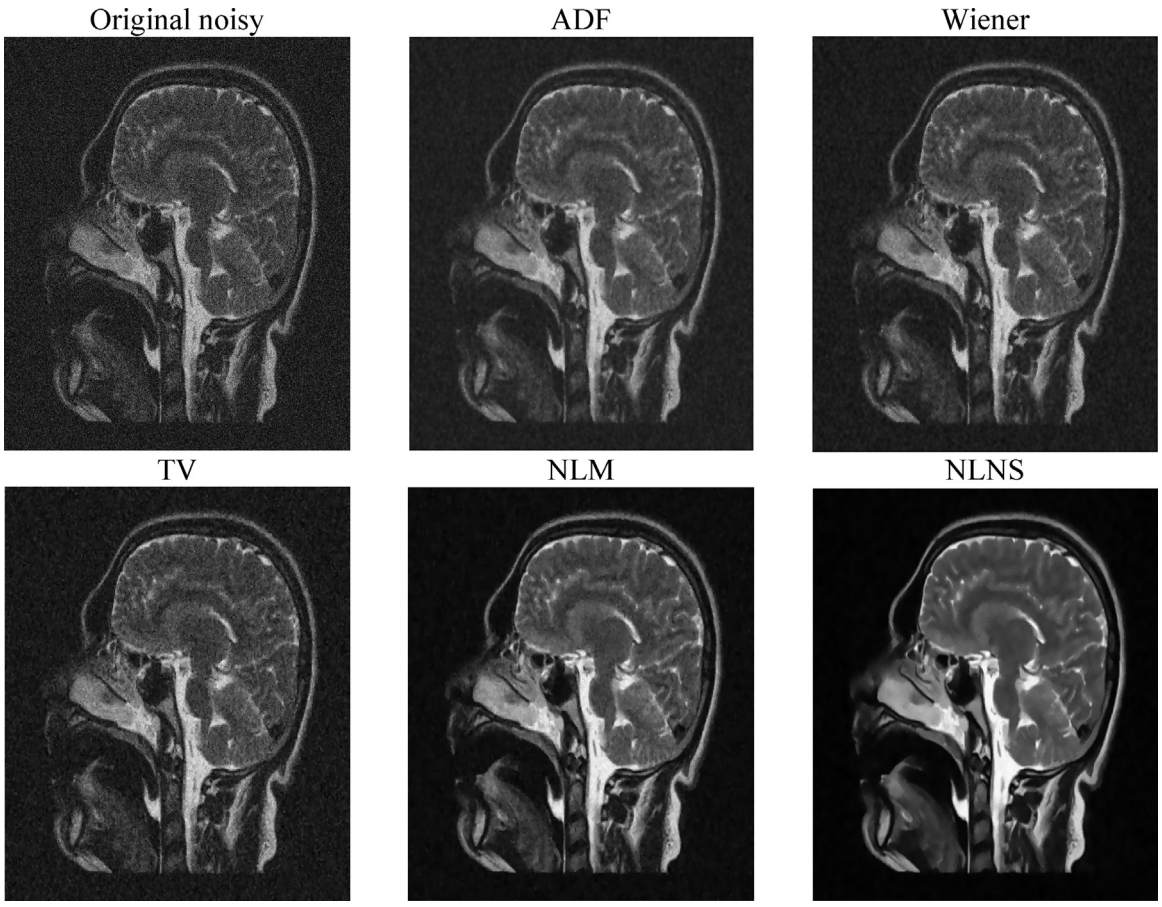

Fig. 6. Denoising results of clinical T2 weighted Sagittal MRI.

The residual image is also obtained by subtracting the denoised image from the noisy image [15]. The residual image is required to verify the traces of anatomical information removed during denoising. Hence, this reveals the excessive smoothing and the blurring of small structural details contained in the image.

4.3. Performance comparison

The performance of the proposed method has been compared with several standard and established algorithms such as Wiener filter, anisotropic diffusion filter, total variation minimization scheme and nonlocal means filter.

4.3.1. Wiener filter

N. Wiener proposed the concept of Wiener filtering also called as minimum mean square error filter or least square error filter in 1942 [36]. This method is founded on considering images and noise as random processes and the objective is to estimate $\hat{f}$ of the uncorrupted image f such that the mean

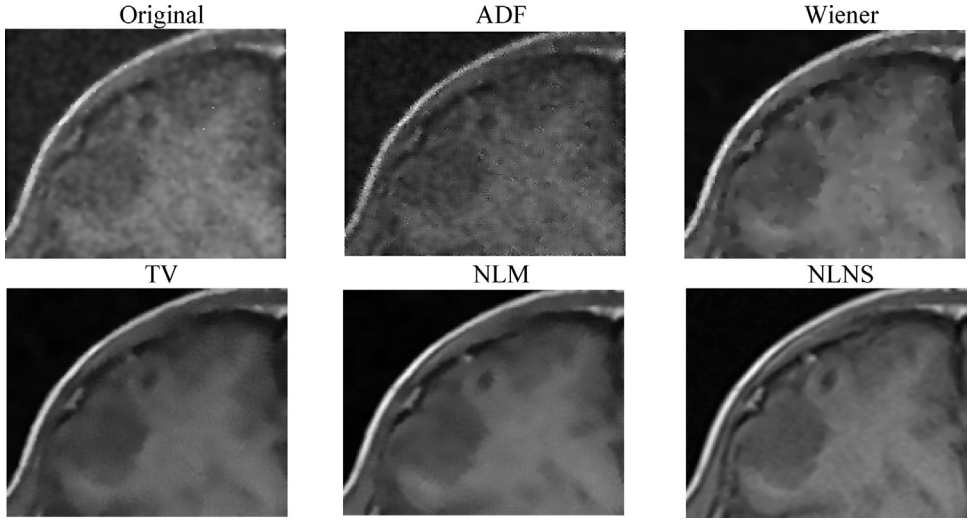

Fig. 7. Denoising results of small part of the clinical T1 weighted axial MRI with tumor pathology.

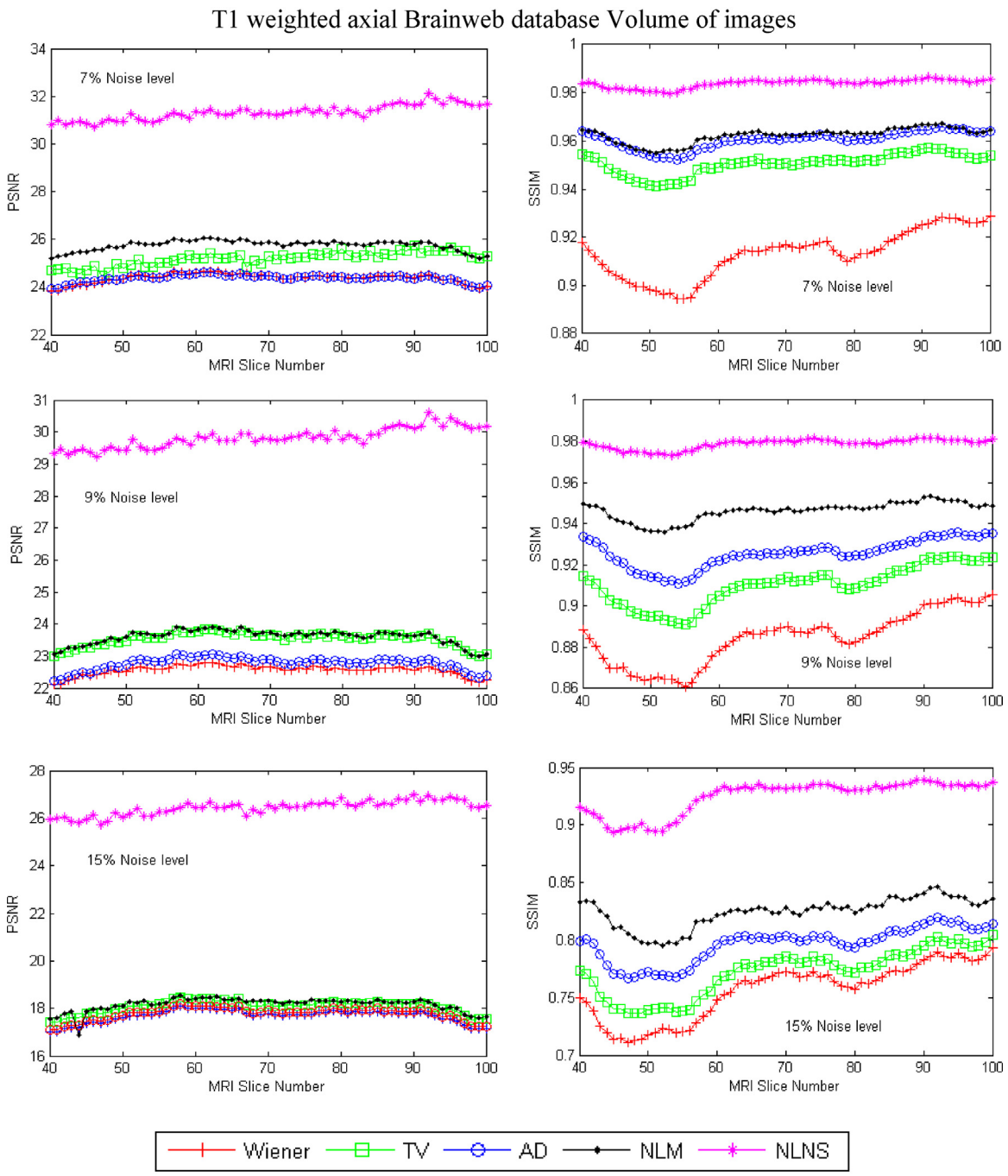

Fig. 8. Results of experiments performed on a sequence of MR images collected from Brainweb MR volume.

square error between them is minimized. This error measure is given by

$$e^2 = E\{(f - \hat{f})^2\} \tag{31}$$

where $E\{\cdot\}$ is the expected value of the argument. In the frequency domain,

$$\hat{F}(u,v) = \left[\frac{H^*(u,v)S_f(u,v)}{S_f(u,v)\left|H(u,v)\right|^2 + S_\eta(u,v)}\right] G(u,v) \tag{32}$$

where $H(u,v)$ is the transform degraded function, $H^*(u,v)$ is the complex conjugate of $H(u,v)$, $S_\eta(u,v)$ is the power spectrum of the noise, $S_f(u,v)$ is the power spectrum of the undegraded image and $G(u,v)$ is the transform of the degraded image. The restored image in the spatial domain is given by the inverse transform of the frequency domain estimate $\hat{F}(u,v)$.

4.3.2. Anisotropic diffusion filter (ADF)

Perona and Malik [37] introduced the anisotropic diffusion filter. In this approach the image u is only convolved in the direction orthogonal to the gradient of the image which ensures the preservation of edges. The iterative denoising process of initial image u_0 can be expressed as

$$\begin{cases} \dfrac{\partial u(x,t)}{\partial t} = div(c(x,t)\nabla u(x,t)) \\ u(x,0) = u_0(x) \end{cases} \tag{33}$$

Table 1
Comparison of the denoising techniques based on the performance metrics for simulated MR images.

MR image	Denoising methods	Performance metrics	
		PSNR (dB)	SSIM
T1-weighted brain MRI corrupted by 7% Rician noise	Wiener	24.4	0.9429
	TV	24.5	0.9540
	ADF	25.3	0.9643
	NLM	25.32	0.9646
	NLNS	31.35	0.9894
T2-weighted brain MRI corrupted by 9% Rician noise	Wiener	22.02	0.8334
	TV	21.58	0.9342
	ADF	22.64	0.9468
	NLM	23.37	0.9494
	NLNS	27.11	0.9813
T1-weighted brain MRI with MS lesion corrupted by 15% Rician noise	Wiener	17.07	0.7870
	TV	16.9	0.7901
	ADF	16.84	0.8127
	NLM	16.88	0.8370
	NLNS	23.92	0.9254

where $\nabla u(x, t)$ is the image gradient at voxel x and iteration t, $\partial u(x, t)/\partial t$ is the partial temporal derivation of $u(x, t)$ and

$$c(x,t) = g(\left|\left|\nabla u(x,t)\right|\right|) = e^{-\|\nabla u(x,t)\|/K^2} \tag{34}$$

where K is the diffusivity parameter.

4.3.3. Total variation (TV) minimization scheme

The difficult task to preserve edges while correctly denoising constant areas has been addressed also by Rudin, Osher and Fatemi. They proposed to minimize the TV norm subject to noise constraints [38], that is

$$\hat{u} = \underset{u\in\Omega^3}{\operatorname{argmin}} \int \left|\nabla u(x,t)\right| \, dx \tag{35}$$

subject to

$$\int_{\Omega^3} (u(x) - u_0(x))\, dx = 0 \quad \text{and} \quad \int_{\Omega^3} \left|u(x) - u_0(x)\right|^2 dx = \sigma^2 \tag{36}$$

where u_0 is the original noisy image, u is the restored image and σ is the standard deviation of the noise. In this model, the TV minimization tends to smooth inside the image structures while keeping the integrity of boundaries. The TV minimization scheme can be expressed as an unconstrained problem

$$\hat{u} = \underset{u\in\Omega^3}{\operatorname{argmin}} \left[\int_{\Omega^3} \left|\nabla u(x)\right| \, dx + \lambda \int_{\Omega^3} \left|u(x) - u_0(x)\right|^2 dx\right] \tag{37}$$

where λ is a Lagrange multiplier which controls the balance between the TV norm and the fidelity term. Thus λ acts as the filtering parameter. Indeed, for high values for λ the fidelity term is encouraged. For small values for λ the regularity term is desired.

All the methods were implemented using MATLAB 2010a (The Math Works, Inc.) in Windows XP 64-bit Edition (Pentium Dual Core 2.4 GHz with 4 GB of RAM). Wiener filtering was computed using the function from Matlab Image Processing Toolbox [39]. For AD filter, the parameter K varies from 0.05 to 1 with a step of 0.05 and the number of iterations varies from 1 to 15. For TV minimization, the parameter λ varies from 0.01 to 1 with step of 0.01 and the number of iterations varies from 1 to 10. There are three key parameters that need to be set to use the NLM filter; one is the size of the search window (w), second one is the size of the neighborhood window (f) and finally, the degree of the filtering (h). For the simulation, the parameters were chosen as $w = 5$, $f = 2$ and h is proportional to the noise level of the image [13].

4.4. Evaluation on simulated data set

The detailed images of the denoising results obtained for the T1 weighted, T2 weighted and T1 weighted with MS lesion axial images corrupted by 7% ($\sigma = 17.36$, PSNR = 20.52 dB), 9% ($\sigma = 22.32$, PSNR = 18.31 dB) and 15% ($\sigma = 37.5$, PSNR = 13.88 dB) of Rician noise respectively shown in Figs. 2–4. From the visual comparison of these results, the proposed method surpassed all other methods at high noise levels on the three types of data in terms of producing more detailed denoised image in which all the distinct features and small structural details are well preserved.

The PSNR and the SSIM values obtained for the T1 weighted, T2 weighted and T1 weighted with MS lesion axial images with different noise levels (1% ($\sigma = 2.5$, PSNR = 37.39 dB) to 15% ($\sigma = 37.5$, PSNR = 13.88 dB)) using the aforementioned denoising techniques are given in Fig. 5. As the level of noise increase, the performance of the proposed NLNS Wiener filter shows significant improvement over the other denoising methods. Table 1 shows a comparison of the experimental results for the denoising methods based on PSNR and SSIM for the T1 weighted, T2 weighted and T1 weighted with MS lesion axial images corrupted by 7%, 9% and 15%, respectively. Higher the value of PSNR and higher the value of SSIM shows that the proposed filter perform superior than the other denoising methods.

4.5. Evaluation on clinical data set

The detailed images of the denoising results obtained for the T2 weighted Sagittal MR image of normal brain are given in Fig. 6. The detailed features and edges in the image are well preserved by the proposed method compared with other denoising methods. The denoising results obtained for the small part of T1 weighted axial brain with tumor pathology are shown in Fig. 7. With the other denoising methods (ADF, Wiener, TV and NLM), the sharpness along the edges and the pathology structure is extensively blurred. Comparing the NLM and NLNS Wiener, it is evident that NLNS Wiener preserves well the details.

4.6. Evaluation on sequence of images

The performance was also evaluated for the sequence volume of MRI scan at the specific intervals in order to take into account the

influence of structural variations of the efficiency of the denoising techniques. The results for the simulated MRI volumes of the T1 weighted slices of 40–100 with 7%, 9% and 15% noise levels, respectively, shown in Fig. 8. It can be noted that the performance of the proposed method is superior to the other denoising techniques.

5. Conclusion

In this paper, a novel MRI denoising technique based on nonlocal neutrosophic set approach of Wiener filtering has been proposed. The method is adapted to Rician noise characteristics. The NLM filtered MR image is described as a NS set using three membership sets *T*, *I* and *F*. The entropy in neutrosophic image domain is defined and employed to measure the indetermination. The Wiener filter is applied to reduce the set's indetermination and to remove the noise in the MR image.

The performance of the proposed denoising filter is compared with Wiener, ADF, TV and NLM based on PSNR and SSIM. The experimental results demonstrate that the proposed approach can remove noise automatically and effectively. This filtering method tends to produce good denoised image not only in terms of visual perception but also in terms of the quality metrics. In the clinical MRI with tumor pathology, the filter preserves the major visual signature of the given pathology. Even though the computational complexity of the proposed method is equal to the NLM filter, on the contrary it increases PSNR and SSIM value of the denoised image. And finally, further works should be implementing spatially adaptive Wiener filtering in the neutrosophic domain for accounting the spatially varying noise level in parallel imaging MRI.

Acknowledgements

The authors would like to acknowledge Dr. Jeny Rajan Assistant Professor, National Institute of Technology, Surathkal, Karnataka, India for his Matlab program to estimate noise in MR images. And also, thank Dr. V. Maheswaran of PSG Institute of Medical Sciences and Research (PSG IMS&R) Coimbatore, Tamilnadu, India for providing us the clinical MRI data and for providing his opinion on the diagnostic details of the denoised images.

References

[1] G. Wright, Magnetic resonance imaging, IEEE Signal Processing Magazine 14 (1997) 56–66.
[2] C.S. Anand, J.S. Sahambi, MRI denoising using bilateral filter in redundant wavelet domain, in: Proc. IEEE Region 10 Conference (TENCON 2008), Hyderabad, India, 2008, pp. 1–6.
[3] R.M. Henkelman, Measurement of signal intensities in the presence of noise in MR images, Medical Physics 12 (1985) 232–233.
[4] E.R. McVeigh, R.M. Henkelman, M.J. Bronskill, Noise and filtration in magnetic resonance imaging, Medical Physics 12 (1985) 586–591.
[5] G. Gerig, O. Kubler, R. Kikinis, F.A. Jolesz, Nonlinear anisotropic filtering of MRI data, IEEE Transactions on Medical Imaging 11 (1992) 221–232.
[6] K. Krissian, S. Aja-Fernández, Noise driven anisotropic diffusion filtering of MRI, IEEE Transactions on Image Processing 18 (2009) 2265–2274.
[7] A. Samsonov, C. Johnson, Noise-adaptive nonlinear diffusion filtering of MR images with spatially varying noise levels, Magnetic Resonance in Medicine 52 (2004) 798–806.
[8] J.B. Weaver, Y. Xu, D.M. Healy, L.D. Cromwell, Filtering noise from images with wavelet transforms, Magnetic Resonance Imaging 21 (1991) 288–295.
[9] R.D. Nowak, Wavelet-based Rician noise removal for magnetic resonance imaging, IEEE Transactions on Image Processing 8 (1999) 1408–1419.
[10] A. Pizurica, W. Philips, I. Lemahieu, M. Acheroy, A versatile wavelet domain noise filtration technique for medical imaging, IEEE Transactions on Medical Imaging 22 (2003) 323–331.
[11] P. Bao, L. Zhang, Noise reduction for magnetic resonance images via adaptive multiscale products thresholding, IEEE Transactions on Medical Imaging 22 (2003) 1089–1099.
[12] X. Yang, B. Fei, A wavelet multiscale denoisng algorithm for magentic resonance images, Measurement Science and Technology 22 (2011) 1–12.
[13] A. Buades, B. Coll, J.M. Morel, A review of image denoising algorithms, with a new one, Multiscale Modeling and Simulation 4 (2005) 490–530.
[14] J.V. Manjon, M. Robles, N.A. Thacker, Multispectral MRI de-noising using non-local means, Medical Image Understanding and Analysis (2007) 41–46.
[15] J.V. Manjón, J. Carbonell-Caballero, J.J. Lull, G. García-Martí, L. Martí-Bonmatí, M. Robles, MRI denoising using non-local means, Medical Image Analysis 12 (2008) 514–523.
[16] P. Coupe, P. Yger, S. Prima, P. Hellier, C. Kervrann, C. Barillot, An optimized blockwise nonlocal means denoising filter for 3-D magnetic resonance images, IEEE Transactions on Medical Imaging 27 (2008) 425–441.
[17] J.V. Manjón, P. Coupe, A. Buades, D.L. Collins, M. Robles, New methods for MRI denoising based on sparseness and self-similarity, Medical Image Analysis 16 (2012) 18–27.
[18] J. Sijbers, A.J. den Dekker, J. Van Audekerke, M. Verhoye, D. Van Dyck, Estimation of the noise in magnitude MR images, Magnetic Resonance Imaging 16 (1998) 87–90.
[19] J. Sijbers, A.J. den Dekker, P. Scheunders, D. Van Dyck, Maximum likelihood estimation of Rician distribution parameters, IEEE Transactions on Medical Imaging 17 (1998) 357–361.
[20] J. Sijbers, A.J. den Dekker, Maximum likelihood estimation of signal amplitude and noise variance form MR data, Magnetic Resonance Imaging 51 (2004) 586–594.
[21] J. Sijbers, D. Poot, A.J. den Dekker, W. Pintjenst, Automatic estimation of the noise variance from the histogram of a magnetic resonance image, Physics in Medicine and Biology 52 (2007) 1335–1348.
[22] L. He, I.R. Greenshields, A nonlocal maximum likelihood estimation method for Rician noise reduction in MR images, IEEE Transactions on Medical Imaging 28 (2009) 165–172.
[23] J. Rajan, D. Poot, J. Juntu, J. Sijbers, Noise measurement from magnitude MRI using local estimates of variance and skewness, Physics in Medicine and Biology 55 (2010) 441–449.
[24] J. Rajan, B. Jeurissen, M. Verhoye, J.V. Audekerke, J. Sijbers, Maximum likelihood estimation-based denoising of magnetic resonance images using restricted local neighborhoods, Physics in Medicine and Biology 56 (2011) 5221–5234.
[25] J. Rajan, J. Veraat, J.V. Audekerke, M. Verhoye, J. Sijbers, Nonlocal maximum likelihood estimation method for denoising multiple-coil magnetic resonance images, Magnetic Resonance Imaging 30 (2012) 1512–1518.
[26] H. Gudbjartsson, S. Patz, The Rician distribution of noisy MRI data, Magnetic Resonance in Medicine 34 (1995) 910–914.
[27] F. Samarandache, A unifying field in logics neutrosophic logic, in: Neutrosophy, Neutrosophic Set, Neutrosophic Probability, 3rd ed., American Research Press, Rehoboth, 2003.
[28] H.D. Cheng, Y. Guo, A new neutrosophic approach to image thresholding, New Mathematics and Natural Computation 4 (2008) 291–308.
[29] Y. Guo, H.D. Cheng, New neutrosophic approach to image segmentation, Pattern Recognition 42 (2009) 587–595.
[30] A. Sengur, Y. Guo, Color texture image segmentation based on neutrosophic set and wavelet transformation, Computer Vision and Image Understanding 115 (2011) 1134–1144.
[31] Y. Guo, H.D. Cheng, Y. Zhang, A new neutrosophic approach to image denoising, New Mathematics and Natural Computation 5 (2009) 653–662.
[32] J. Mohan, V. Krishnaveni, Y. Guo, A neutrosophic approach of MRI denoising, in: Proc. IEEE International Conference on Image Information Processing, Shimla, India, 2011, pp. 1–6.
[33] J. Mohan, V. Krishnaveni, Y. Guo, J. Kanchana, MRI denoising based on neutrosophic Wiener filtering, in: Proc. IEEE International Conference on Imaging Systems and Techniques (IST 2012), Manchester, United Kingdom, 2012, pp. 327–331.
[34] R.K. Kwan, A.C. Evans, G.B. Pike, MRI simulation based evaluation of image processing and classification methods, IEEE Transactions on Medical Imaging 18 (1999) 1085–1097.
[35] Z. Wang, A.C. Bovik, H.R. Sheikh, E.P. Simoncell, Image quality assessment: from error visibility to structural similarity, IEEE Transactions on Image Processing 13 (2004) 600–612.
[36] R.C. Gonzalez, R.E. Woods, Digital Image Processing, 2nd ed., Pearson Education, India, 2002.
[37] P. Perona, J. Malik, Scale-space and edge detection using anisotropic diffusion, IEEE Transactions on Pattern Analysis and Machine Intelligence 12 (1990) 629–639.
[38] L.I. Rudin, S. Osher, E. Fatemi, Nonlinear total variation based noise removal algorithms, Physica D 60 (1992) 259–268.
[39] Mathworks, The Matlab Image Processing Toolbox, http://www.mathworks.com/access/helpdesk/help/toolbox/images/

J. Mohan received the BE (ECE) degree from Bharathidasan University, Trichy and ME degree from Sathyabama University, Chennai. Currently pursuing his PhD in medical image processing in PSG College of Technology, Anna University, Chennai. Presently working as an assistant professor at P.A. College of Engineering and Technology with an experience of 11 years in the teaching field.

Dr. **V. Krishnaveni** is associate professor in the department of electronics and communication engineering, PSG College of Technology, Coimbatore. She did her BE (ECE) and ME (communication systems) from Bharathiar University, Coimbatore and PhD in the area of biomedical signal processing from Anna University Chennai. She has more than 15 years of teaching experience at UG and PG levels. She has published more than 25 papers in various international/national journals/conferences. She is a reviewer for more than 5 international journals which includes *IEEE Transactions on Biomedical Engineering*. Her research interests include digital signal processing and image processing with applications to biomedical signals and images.

Dr. **Yanhui Guo** is currently working in the School of Science, Technology and Engineering Management, Saint Thomas University, Miami Gardens, USA. He received BS degree in automatic control from Zhengzhou University, PR China, in 1999, the MS degree in pattern recognition and intelligence system from Harbin Institute of Technology, Harbin, Heilongjiang Province, PR China, in 2002, and the PhD degree in the department of computer science, Utah State University, USA, in 2010. His research interests include image processing, pattern recognition, medical image processing, computer-aided detection/diagnosis, fuzzy logic, and neutrosophic theory.